Pressure-induced monoclinic distortion and charge and orbital ordering in $La_{0.5}Ca_{0.5}MnO_3$

D. P. Kozlenko,[1] L. S. Dubrovinsky,[2] I. N. Goncharenko,[3] B. N. Savenko,[1] V. I. Voronin,[4] E. A. Kiselev,[4] and N. V. Proskurnina[4]

[1]*Frank Laboratory of Neutron Physics, JINR, 141980 Dubna, Russia*
[2]*Bayerisches Geoinstitut, Univesität Bayreuth, Bayreuth D-95440, Germany*
[3]*Laboratoire Léon Brillouin, CEA-CNRS, CE Saclay, 91191 Gif-sur-Yvette, France*
[4]*Institute for Metal Physics, Ural Division of RAS, 620219 Yekaterinburg, Russia*

(Received 11 December 2006; published 12 March 2007)

The crystal structure, Raman spectra, and magnetic structure of $La_{0.5}Ca_{0.5}MnO_3$ were studied at high pressures up to 31 and 6.2 GPa. A structural transition from orthorhombic to monoclinic phase was found at $P \sim 15$ GPa and room temperature. The charge-exchange-type antiferromagnetic ground state is stable under pressure with $dT_N/dP \approx 4$ K/GPa. Unlike other half-doped systems $Pr_{0.5}Sr_{0.5}MnO_3$, $Nd_{0.5}Sr_{0.5}MnO_3$, and also $LaMnO_3$ exhibiting pressure-induced metallization, in $La_{0.5}Ca_{0.5}MnO_3$ the opposite tendency to pressure-induced charge localization occurs, caused by development of monoclinic distortion due to charge and orbital ordering.

DOI: 10.1103/PhysRevB.75.104408 PACS number(s): 75.25.+z, 61.50.Ks, 71.30.+h, 78.30.−j

I. INTRODUCTION

Perovskite manganites $R_{1-x}A_xMnO_3$ (R, rare-earth element; A, alkali-earth element) exhibit a rich variety of fascinating physical phenomena extensively studied in the recent years—colossal magnetoresistance, charge and orbital ordering, and mesoscopic phase separation.[1,2] A complicated balance of ferromagnetic (FM) double exchange mediated by charge carriers of e_g nature and antiferromagnetic (AFM) superexchange interactions between localized magnetic moments of t_{2g} nature coupled to lattice distortion effects and orbital degrees of freedom leads to especially complex phase diagram of compounds with $x \sim 0.5$, the value located at phase boundaries between insulating and metallic states and also states with different magnetic order.

The properties of half-doped manganites depend substantially on the distortion of Mn^{3+}-O^{2-}-Mn^{4+} network, which can be mediated by variation of the average A-site ionic radius $\langle r_A \rangle$ or high pressure. In $La_{0.5}Sr_{0.5}MnO_3$ and $Pr_{0.5}Sr_{0.5}MnO_3$ compounds with a larger $\langle r_A \rangle$, the metallic conductivity and layered A-type AFM state with $d(x^2-z^2)$ e_g orbital order (OO) occur at ambient pressure.[3,4] In $Nd_{0.5}Ca_{0.5}MnO_3$, $Pr_{0.5}Ca_{0.5}MnO_3$, $La_{0.5}Ca_{0.5}MnO_3$, and $Nd_{0.5}Sr_{0.5}MnO_3$ with a smaller $\langle r_A \rangle$, a charge ordered (CO) insulating ground state with $d(x^2-r^2)/d(3z^2-r^2)$ e_g orbital order occurs, in which Mn^{3+} and Mn^{4+} ions form two-sublattice charge-exchange (CE)-type AFM structure with propagation vectors $k_C=(1/2\ 0\ 1/2)$ and $k_E=(0\ 0\ 1/2)$.[5–9]

Recently a pressure-induced suppression of the insulating CE-type AFM ground state in favor of the metallic A-type AFM state was observed in $Nd_{0.5}Sr_{0.5}MnO_3$ at $P \sim 3.5$ GPa.[10,11] In $Pr_{0.5}Sr_{0.5}MnO_3$, the metallic A-type AFM state region gets enhanced due to substantial increase of T_N under pressure.[12] The metallization at $P \sim 32$ GPa and suppression of orbital ordering at $P \sim 18$ GPa occur in undoped $LaMnO_3$.[13] In contrast, the shear strain evolution in $Nd_{0.5}Ca_{0.5}MnO_3$ up to 15 GPa, evidenced from x-ray diffraction study, assumes the stability of the insulating state under pressure.[14] These observations imply the presence of competing charge delocalization and localization tendencies in half-doped manganites with different $\langle r_A \rangle$ at high pressures.

An assumption about possible pressure-induced charge localization in compounds with small $\langle r_A \rangle$ clearly needs further clarification and requires more detailed investigations of structural and physical properties, especially taking into account that most previous investigations were performed in the restricted pressure range up to 15 GPa only. For this purpose, we have studied $La_{0.5}Ca_{0.5}MnO_3$ compound with intermediate $\langle r_A \rangle$ between $Nd_{0.5}Sr_{0.5}MnO_3$ and $Nd_{0.5}Ca_{0.5}MnO_3$ by means of x-ray, neutron-diffraction, and Raman spectroscopies in extended pressure range up to 31 GPa.

II. EXPERIMENT

A $La_{0.5}Ca_{0.5}MnO_3$ polycrystalline sample was obtained using the standard solid-state reaction method. The initial reagents were La_2O_3, $CaCO_3$, and MnO_2. La_2O_3 was preliminarily annealed at 1200 °C for 2 h, $CaCO_3$ at 500 °C for 3 h, and MnO_2 at 750 °C for 24 h. The latter process involved the transition from MnO_2 to Mn_2O_3. A mixture of the oxides was taken in the necessary stoichiometric proportion and thoroughly ground in ethanol. The mixture was annealed in four steps with intermediate grinding in ethanol every 20 h: the first stage was annealing at 850 °C for 20 h; the second stage, at 950 °C for 20 h; the third stage, at 1100 °C for 100 h; and the fourth stage, at 1200 °C for 200 h. Then, the sample was quenched by cooling to room temperature.

X-ray powder diffraction and Raman spectroscopy measurements of $La_{0.5}Ca_{0.5}MnO_3$ were made at high pressures up to 31 GPa and ambient temperature with a diamond-anvil cell.[15] The sample was loaded in the steel gasket with a 4:1 methanol-ethanol mixture as a pressure-transmitting medium. The pressure was measured using the ruby fluorescence technique. The x-ray diffraction spectra were measured at the system consisting of high-brilliance FRD rotating anode generator (Mo $K\alpha$ radiation, $\lambda=0.7115$ Å), FluxMax focusing optics, and Bruker APEX charge-coupled device area detector. The two-dimensional XRD images were

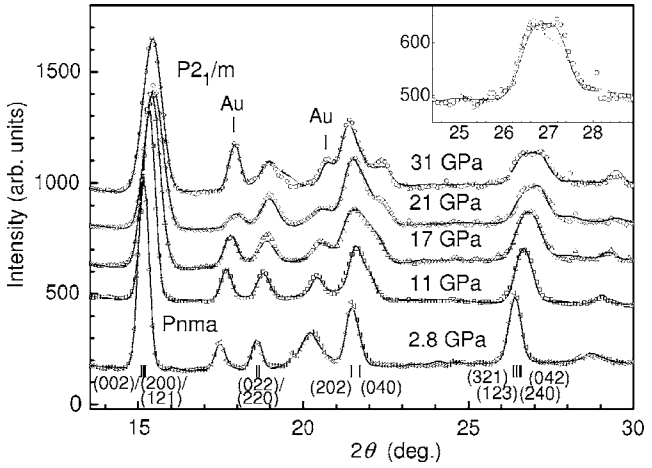

FIG. 1. X-ray diffraction patterns of $La_{0.5}Ca_{0.5}MnO_3$ measured at selected pressures and ambient temperature and processed by the Rietveld method. Experimental points and calculated profiles are shown. A thin piece of Au wire was added to the sample as x-ray pressure marker. The dashed and solid lines in the inset correspond to the calculated diffraction patterns in the orthorhombic *Pnma* and monoclinic $P2_1/m$ structural models.

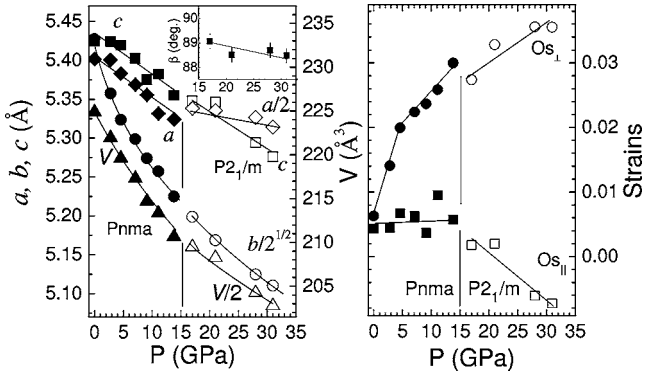

FIG. 2. Lattice parameters, unit-cell volume, and orthorhombic strains in $La_{0.5}Ca_{0.5}MnO_3$ as functions of pressure.

converted to conventional one-dimensional diffraction patterns using FIT2D program.[16] The data analysis was performed using GSAS program.[17]

Raman spectra were collected using LabRam spectrometer (NeHe excitation laser with wavelength of 632 nm, grating of 1800, confocal hole of 11 μm, 50× objective, and power of 25 mW).

The magnetic structure of $La_{0.5}Ca_{0.5}MnO_3$ was investigated with the G6.1 diffractometer at the Orphée reactor (Laboratoire Léon Brillouin, France). The incident neutron wavelength was 4.74 Å. The sample with a volume of about 1 mm^3 was loaded in the sapphire anvil high-pressure cell.[18] As a pressure-transmitting medium, NaCl was admixed to the sample in 1:2 volume proportion. The pressure was measured by the ruby fluorescence technique. Neutron focusing systems[19] and special cadmium protection were used to increase neutron flux at the sample position and achieve low background level, respectively. The measurements were performed in the pressure range of 0–6.2 GPa and temperature range of 1.5–300 K. The diffraction data were analyzed by the Rietveld method using the FULLPROF program.[20]

III. RESULTS AND DISCUSSION

At ambient conditions, $La_{0.5}Ca_{0.5}MnO_3$ has an orthorhombically distorted perovskite crystal structure (space group *Pnma*) with lattice parameters related to those of the ideal cubic subcell as $a \approx c \approx a_p\sqrt{2}$ and $b \approx 2a_p$.[7,8] Due to a pseudocubic character of the lattice, x-ray diffraction patterns at ambient conditions have rather symmetric peaks (Fig. 1). With a pressure increase up to 15 GPa, the diffraction peak formed by (202) and (040) reflections and located at $2\theta = 21.5°$ splits into two peaks whose intensities are scaled approximately as 2:1 (Fig. 1). The calculated intensity ratio for (202) and (040) reflections is also about 2:1, and such a splitting indicates an anisotropic compression with noticeably larger compressibility of the *b* lattice parameter in comparison with *a* and *c* ones (Fig. 2). The compression anisotropy can be characterized by "orthorhombic" strains $Os_{\parallel} = 2(c-a)/(c+a)$ in the (*ac*) plane and $Os_{\perp} = 2(a+c-b\sqrt{2})/(a+c+b\sqrt{2})$ along the *b* axis.[21] The $Os_{\perp}$ does not follow a simple linear law and exhibits a slope change at $P \sim 5$ GPa, while the $Os_{\parallel}$ increases slightly with a pressure increase (Fig. 2). The peculiar pressure behavior of orthorhombic strains was also observed in $La_{0.75}Ca_{0.25}MnO_3$,[21] $Nd_{0.45}Sr_{0.55}MnO_3$,[10] and $Nd_{0.5}Ca_{0.5}MnO_3$ (Ref. 14). The unit-cell volume versus pressure dependence does not show any signatures (Fig. 2). The volume compressibility data of $La_{0.5}Co_{0.5}MnO_3$ (Fig. 2) were fitted by the third-order Birch-Murnaghan equation of state:[22]

$$P = \frac{3}{2}B_0(x^{-7/3} - x^{-5/3})\left[1 + \frac{3}{4}(B' - 4)(x^{-2/3} - 1)\right],$$

where $x = V/V_0$ is the relative volume change, V_0 is the unit-cell volume at $P=0$, and B_0 and B' are the bulk modulus $[B_0 = -V(dP/dV)_T]$ and its pressure derivative $[B' = (dB_0/dP)_T]$. The value $B_0 = 186(5)$ GPa calculated with the fixed $B' = 8.5$ found for $LaMnO_3$ (Ref. 13) is comparable with that of 172 GPa obtained for $Nd_{0.5}Ca_{0.5}MnO_3$ (Ref. 14) and larger than $B_0 = 108$ GPa for $LaMnO_3$.[13]

Raman spectra of $La_{0.5}Ca_{0.5}MnO_3$ at high pressures up to 15 GPa exhibit peaks located at ~227, 245, 420, and 445 cm^{-1} (Fig. 3). They can be assigned to the in-phase rotational mode of MnO_6 octahedra around the *b* axis with A_g character, mixed out-of-phase rotational mode of MnO_6 octahedra, so-called "tilt" mode, containing contributions with A_g and B_{1g} character, and out-of-phase apical oxygen bending modes of B_{1g} and A_g character, respectively.[23–26] The modes with A_g and B_{1g} character correspond to the same rotations around the *a* and *c* axes and they are expected to be similar in frequency. In the *Pnma* orthorhombic structure, there are two tilt angles of MnO_6 octahedra, $\varphi_1 = (1/2) \times (\pi\text{-[Mn-O1-Mn]})$ with respect to (010) direction formed by apical Mn-O1 bonds oriented along the *b* axis and $\varphi_2 = (1/2)(\pi\text{-[Mn-O2-Mn]})$ with respect to (101) direction formed by two pairs of nonequivalent Mn-O2 bonds located within the *ac* plane. The rotational and tilt modes are sensi-

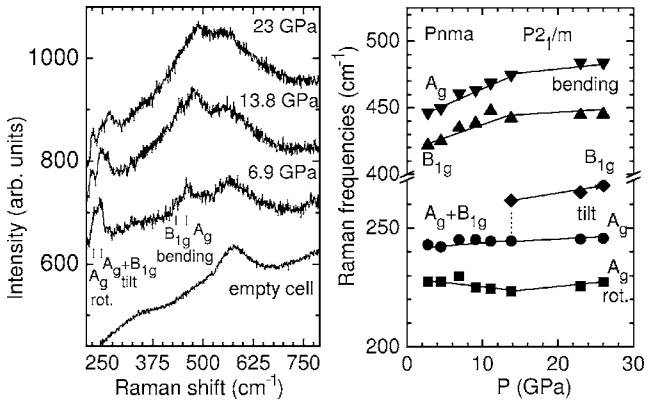

FIG. 3. Raman spectra at selected pressures (left) and pressure dependences of rotational, tilt, and bending modes (right) in $La_{0.5}Ca_{0.5}MnO_3$ at ambient temperature.

tive to the variation of the φ_1 and φ_2 tilt angles,[23,24,26] while bending mode is sensitive to the variation of the average of short La-O distances.[23]

In the pressure range up to 15 GPa, the rotational mode frequency exhibits a slight decrease, the tilt one a slight increase, and the B_{1g} and A_g bending modes a more substantial increase (Fig. 3). It reflects the slight decrease of the φ_2 and increase of the φ_1 tilt angles and the more significant reduction of short La-O1 distances. Such structural changes are similar to those found for the relevant compound $Pr_{0.75}Na_{0.25}MnO_3$ (each Na^+ ion creates two Mn^{4+} ions) from neutron diffraction.[27] More pronounced variation of bending mode in comparison with rotational mode frequencies under pressure was also found for $La_{0.75}Ca_{0.25}MnO_3$.[28] One should note that the structural response of perovskitelike oxides to high pressure in terms of octahedral tilting depends strongly on the A-site ionic radius, as has been shown for $RAlO_3$ and other related compounds.[29,30] The calculated Grüneisen parameters $\gamma_i = -\partial(\ln \nu_i)/\partial \ln V$ are -0.3 for the rotational mode, 0.2 for the tilt mode, and 0.8 and 1.0 for B_{1g} and A_g bending modes, respectively.

At ambient pressure, the MnO_6 octahedra in $La_{0.5}Ca_{0.5}MnO_3$ are nearly isotropic with approximately equal Mn-O1,2 bond lengths.[7,8] The rapid compression of the crystallographic b axis leads to the apical contraction of MnO_6 octahedra with short Mn-O1 and long Mn-O2 bond lengths. In manganites a direct relationship between the distortion of MnO_6 octahedra and orbital ordering exists since half-filled e_g orbitals of Mn^{3+} ions tend to locate at the long Mn-O distance.[1,2,9,31] The pronounced compression anisotropy should result in the electronic density redistribution caused by the gradual increase of the e_g orbital population in the ac plane at the expense of that along the b-axis direction. This process seems to be completed at $P \sim 5$ GPa, where the compressibility of the b axis decreases noticeably (Fig. 2), and at higher pressures, the majority of half-filled e_g orbitals is expected to locate in the ac planes.

At $P \sim 17$ GPa, an additional splitting of the peak located at $2\theta \approx 26.5°$ appears in x-ray diffraction spectra (Fig. 1). With further pressure increase, it becomes more significant and results in considerable redistribution of diffraction intensity in the broad 2θ range of 26°–28°. Such changes in diffraction patterns could not be reproduced consistently in the orthorhombic $Pnma$ symmetry and manifest the pressure-induced structural phase transition. Since other diffraction peaks do not show pronounced changes, the observed splitting of the peak at $2\theta \approx 26.5°$ can be an indicator of the crystal symmetry lowering.

At ambient pressure, the appearance of orbital and charge ordering in $La_{0.5}Ca_{0.5}MnO_3$ is accompanied by the monoclinic distortion of the Mn^{4+} sublattice associated with the enhanced localization of the e_g electrons at Mn^{3+} sublattice, as well as the apical contraction of MnO_6 octahedra. For ambient conditions in bulk $La_{0.5}Ca_{0.5}MnO_3$, short-range charge ordering fluctuations are very strong, as evident from optical spectroscopy,[32] while in thin films the long-range charge ordering occurs.[33] As the pressure-induced anisotropic compression of MnO_6 octahedra is identical to one associated with the appearance of the monoclinic orbital and charge long-range ordered state at ambient pressure and low temperatures, one may suggest that observed changes in x-ray diffraction spectra correspond to the formation of a similar state at high pressure and ambient temperature. Possible structural models of the monoclinic OO CO state in $La_{0.5}Ca_{0.5}MnO_3$ were recently considered in Ref. 34. The model with the $P2_1/m$ symmetry and doubling of the unit cell along the a axis was found to give the best description of the experimental data at $P=0$.[34] We found that such a monoclinic model fits well and considerably better than the orthorhombic one, our diffraction data at $P \geqslant 17$ GPa (Fig. 1).

In the monoclinic phase, the pressure-induced lattice distortion evolves in all three dimensions upon compression, as it comes from pronounced changes of both $Os_\perp$ and $Os_\parallel$ strains (Fig. 2). In comparison with the orthorhombic phase, the bulk modulus (also calculated with $B'=8.5$) increases noticeably to 274(5) GPa, while the unit-cell volume per formula unit extrapolated to zero pressure decreases by 2%.

Raman spectra of the monoclinic phase resemble those of the orthorhombic one (Fig. 3). The only feature is the splitting of the peak corresponding to the tilt mode frequencies of A_g and B_{1g} character caused by the different compressibilities of a and c axes, making these directions less equivalent. Due to close atomic arrangement in orthorhombic and monoclinic phases, it was shown that the mode assignment can be done on the basis of the simplified orthorhombic structure (the monoclinic angle is close to 90°).[25] The obtained Grüneisen parameters are 0.4 for the rotational mode, 0.2 and 0.4 for the B_{1g} and A_g tilt modes, and 0.3 and 0.4 for B_{1g} and A_g bending modes, respectively. The difference in γ_i values for the modes with B_{1g} and A_g character is related to the anisotropic compression of the lattice. We also observed an increase of the Raman mode intensity in the 450–650 cm^{-1} region (Fig. 3). This is expected due to the intensity increase of stretching modes located at ~490 and 615 cm^{-1} (at $P=0$), caused by the onset of charge and orbital ordering.[25,26] These modes, however, are known to be weak in intensity at ambient conditions, and due to excessive peak overlap at high pressures, it was difficult to determine their frequencies accurately.

The increase of the observed Raman mode frequencies in the monoclinic phase (Fig. 3) implies the increase of tilt angles and decrease of the La-O short lengths under pressure.

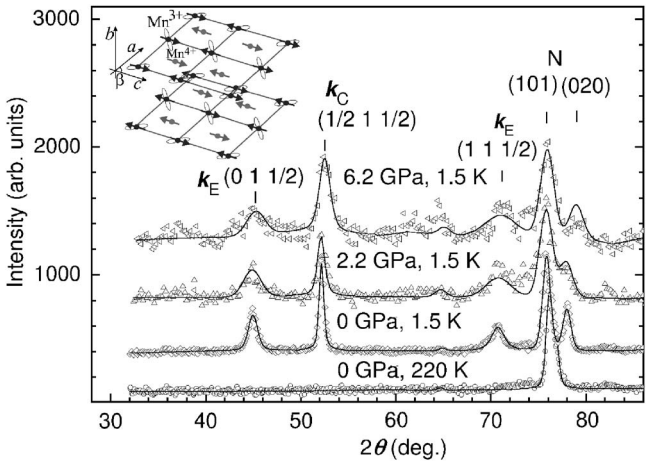

FIG. 4. Neutron-diffraction patterns of $La_{0.5}Ca_{0.5}MnO_3$ measured at different pressures and temperatures and processed by the Rietveld method. The CE-type AFM structure and characteristic $d(3x^2-r^2)/d(3z^2-r^2)e_g$ orbital order of Mn^{3+} sublattice are also shown.

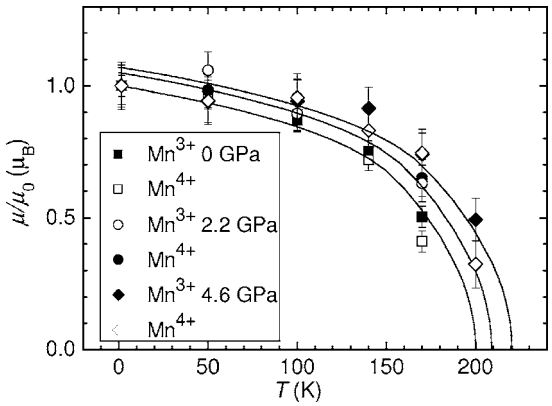

FIG. 5. Temperature dependences of magnetic moments of Mn^{3+} and Mn^{4+} magnetic sublattices of the CE-type AFM state of $La_{0.5}Ca_{0.5}MnO_3$ at different pressures normalized to the values obtained at $P=0$.

It should result in the enhanced charge localization as expected for the CO OO state, since the e_g electron transfer integral in Mn^{3+}-O^{2-}-Mn^{4+} network varies with tilt angles as $t_i \sim \cos\varphi_i$.[1,35]

For an additional insight into the nature of the observed monoclinic phase in $La_{0.5}Ca_{0.5}MnO_3$, we have performed investigations of its magnetic structure at high pressures by neutron diffraction. The measurements were performed by increasing temperature from 1.5 K. In the entire studied pressure range up to 6.2 GPa, below $T_N \sim 200$ K, a typical pattern corresponding to the appearance of the CE-type AFM structure[7,8] with propagation vectors $k_E=(0\ 0\ 1/2)$ and $k_C=(1/2\ 0\ 1/2)$ was observed (Fig. 4). In this magnetic structure, Mn magnetic moments locate in the (ac) planes and form quasi-one-dimensional ferromagnetic zigzag chains-Mn^{3+}-O-Mn^{4+}-with an AFM interchain coupling. Their values at $T=1.5$ K, $\mu_{Mn^{3+}}=2.3(1)\mu_B$ and $\mu_{Mn^{4+}}=2.1(1)\mu_B$, are similar to those obtained at ambient pressure in Refs. 7 and 8 and remain nearly unchanged under high pressure. The formation of the CO OO CE-type AFM state is associated with a noticeable pseudotetragonal apical compression of the unit cell and MnO_6 octahedra along the b axis, as can be seen from the splitting between (101) and (020) nuclear peaks (Fig. 4). It can be characterized by the pseudotetragonal distortion parameter $s=b\sqrt{2}/(a+c)$, the value of which increases from 0.976 to 0.967 in the pressure range of 0–6.2 GPa at 1.5 K. For a comparison, the s values estimated from x-ray diffraction data at $T=290$ K are 0.999 and 0.985 for 0 and 6.2 GPa, respectively. Above T_N an additional magnetic contribution to the nuclear peaks (101)(020) was found, which is relevant to the formation of the intermediate FM state with $T_C \sim 240$ K.[7,25]

The Neel temperature increases nearly linearly with $dT_N/dP=4(1)$ K/GPa, as estimated from temperature dependences of magnetic moments (Fig. 5). Extrapolating to higher pressures, we can estimate the $T_N \sim 270$ K for $P \sim 17$ GPa. At ambient pressure in half-doped manganites, generally T_{CO} exceeds T_N by ~ 20 K.[1,2,5–9] For the small pressures, one can estimate the value $dT_{CO}/dP \sim 3.3$ K/GPa from the Ehrenfest relation $dT_{CO}/dP = VT\Delta\alpha/\Delta C_p$ and known ambient pressure thermal expansion and heat capacity data.[7,36] The averaged per 0–17 GPa pressure range value $dT_{CO}/dP \sim 6$ K/GPa corresponding to observation of the monoclinic phase at ambient temperature is somewhat larger. Nevertheless, both estimations are comparable with dT_N/dP, implying that characteristic temperatures of CO OO and magnetic ordering change accordingly under pressure. An increase of magnetic and charge ordering temperatures under pressure with close pressure coefficients was also observed for lightly doped compound $La_{1-x}Sr_xMnO_3$ ($x \sim 1/8$) with a ferromagnetic ground state and orbital polaron lattice.[37]

Let us compare the pressure behavior of compounds with different $\langle r_A \rangle$ values. In $Pr_{0.5}Sr_{0.5}MnO_3$ ($\langle r_A \rangle = 1.245$ Å) the average tilt angle is small, $\varphi \approx 5°$. The ground layered A-type AFM metallic state is stable at $P=0$ and its region in the phase diagram gets enhanced at high pressures.[12] For $Nd_{0.5}Sr_{0.5}MnO_3$ ($\langle r_A \rangle = 1.237$ Å), the $\varphi \approx 6°$ value is slightly larger than that for $Pr_{0.5}Sr_{0.5}MnO_3$, but it exhibits the insulating CO OO CE-type AFM ground state.[9–11] The resistivity is of polaronic character and activation energy is very small, $E_a \approx 2$ meV, indicating weak electron-phonon coupling.[9–11] It can be related to the polaron binding energy approximately as $E_a \approx (1/2)E_{JT}$.[38] Neglecting the electron-phonon coupling, one can estimate quite similar charge carrier bandwidths[35] $W \sim t \sim \cos(\varphi)/l^{3.5}$ in $Nd_{0.5}Sr_{0.5}MnO_3$ and $Pr_{0.5}Sr_{0.5}MnO_3$, with close average tilt angles and Mn-O bond lengths l.

Appearance of the A-type AFM state in $Nd_{0.5}Sr_{0.5}MnO_3$ and its stability in $Pr_{0.5}Sr_{0.5}MnO_3$ under pressure can be explained in terms of the simple degenerate double-exchange model[39] incorporating the superexchange AFM interaction J_{AF} between localized t_{2g} spins and FM double exchange mediated by delocalized e_g electrons and controlled by the electron transfer integral t, with Hund's coupling $J_H \gg t$. Due to a stronger pressure dependence[12,40] of $J_{AF} \sim l^{-14}$ over $t \sim l^{-3.5}$, the balance J_{AF}/t is changed in favor of J_{AF} upon compression, leading to the stabilization of the A-type AFM

state.[12] In the A-type AFM state with characteristic $d(x^2-z^2)e_g$ orbital order, the electron transfer is allowed within planes with FM ordering of Mn ions, leading to a higher possible kinetic-energy gain in comparison with the CE-type AFM state, where such a transfer is possible along quasi-one-dimensional zigzag Mn^{3+}-O^{2-}-Mn^{4+} FM chains only.[1,2,9]

In $La_{0.5}Ca_{0.5}MnO_3$ ($\langle r_A\rangle = 1.198$ Å), the initial $\varphi \approx 10°$ value is about twice[7] and $E_a \sim 100$ meV 2 orders of magnitude larger[41] in comparison with $R_{0.5}Sr_{0.5}MnO_3$ (R=Pr,Nd), although Mn-O distances are comparable. The e_g electron localization and electron-phonon coupling become much more pronounced, leading to the bandwidth reduction[42] to $W = W_0 \exp(-gE_{JT}/\hbar\omega)$, where ω is the characteristic phonon frequency and parameter $0 < g < 1$ depends on $E_{JT}/\hbar\omega$. With $\omega \sim 75$ meV (Refs. 25 and 26) and $g \sim 0.5$, one can estimate $W_{LaCa} \sim 0.25 W_{RSr}$ (R=Pr,Nd).

Theoretically it was shown that the appearance of the CO OO CE-type AFM ground state in half-doped manganites with smaller $\langle r_A\rangle$ could not be reproduced in the simple double-exchange model discussed above and suitable for the case of large bandwidth compounds, and one needs to introduce additional terms for its description. In particular, the important role of electron-phonon coupling,[43–45] on-site[46] and intersite[47] Coulomb interactions, and specific topology of FM zigzag chains[48] in the CE-type AFM state was assumed. The introduction of electron-phonon coupling terms due to cooperative or noncooperative Jahn-Teller (JT) phonons was found to be sufficient for the construction of the phase diagram of half-doped manganites with CO OO CE-type AFM state and consideration of Coulomb interactions gives no qualitative difference.[44,45]

According to the theoretical phase diagram,[45] for the intermediate electron-phonon coupling strength, the increase of T_N and T_{CO} is expected with the increase of the J_{AF}/t ratio. Hence, the pressure-induced increase of J_{AF}/t upon Mn-O bond length compression is expected to cause the increase of T_N and T_{CO}, in agreement with the present experimental observation in $La_{0.5}Ca_{0.5}MnO_3$. The monoclinic distortion evolving under pressure in $La_{0.5}Ca_{0.5}MnO_3$ due to the development of the CO OO state with CE-type AFM order should also result in the enhancement of electron-phonon coupling and charge localization, and subsequently, in the further stabilization of the CO OO state.

Although we were unable to evaluate shear strains of MnO_6 octahedra due to difficulties with accurate oxygen coordinate determination, the pressure behavior of shear strains found for $Nda_{0.5}Ca_{0.5}MnO_3$ up to 15 GPa (Ref. 14) is compatible with the observed decrease of the φ_2 and increase of the φ_1 tilt angles in the orthorhombic phase of $La_{0.5}Ca_{0.5}MnO_3$.

IV. CONCLUSIONS

Our results demonstrate that half-doped manganites with large and small $\langle r_A\rangle$ values exhibit drastically different behaviors under high pressure. In $Pr_{0.5}Sr_{0.5}MnO_3$, $Nd_{0.5}Sr_{0.5}MnO_3$, and likely $La_{0.5}Sr_{0.5}MnO_3$ with a relatively large $\langle r_A\rangle$ and charge carrier bandwidth, the electron-phonon coupling effects are negligible and the competing balance between the AFM superexchange and FM double-exchange interactions with increasing J_{AF}/t ratio leads to the stabilization of the A-type AFM metallic state under pressure. In contrast, due to the presence of the pronounced electron-phonon coupling and charge localization in compounds with smaller $\langle r_A\rangle$ and bandwidth, e.g., $La_{0.5}Ca_{0.5}MnO_3$, $Nd_{0.5}Ca_{0.5}MnO_3$, and likely $Pr_{0.5}Ca_{0.5}MnO_3$, the stabilization of the CO OO CE-type AFM insulating state occurs under pressure. Subsequently, a significant pressure-induced lattice distortion is developed, which should result in the additional enhancement of electron-phonon coupling and charge localization.

ACKNOWLEDGMENTS

The allocation of beam time and financial support of the BGI and LLB facilities and the Russian Foundation for Basic Research, Grant No. 06-02-81018-Bel-a, are gratefully acknowledged.

[1] *Colossal Magnetoresistance Oxides*, edited by Y. Tokura (Gordon and Breach, New York, 2000).
[2] E. Dagotto, T. Hotta, and A. Moreo, Phys. Rep. **344**, 1 (2001).
[3] O. Chmaissem, B. Dabrowski, S. Kolesnik, J. Mais, J. D. Jorgensen, and S. Short, Phys. Rev. B **67**, 094431 (2003).
[4] F. Damay, C. Martin, M. Hervieu, A. Maignan, B. Raveau, G. André, and F. Boureé, J. Magn. Magn. Mater. **184**, 71 (1998).
[5] F. Millange, S. de Brion, and G. Chouteau, Phys. Rev. B **62**, 5619 (2000).
[6] Z. Jirák, F. Damay, M. Hervieu, C. Martin, B. Raveau, G. André, and F. Bourée, Phys. Rev. B **61**, 1181 (2000).
[7] P. G. Radaelli, D. E. Cox, M. Marezio, and S.-W. Cheong, Phys. Rev. B **55**, 3015 (1997).
[8] M. Pissas and G. Kallias, Phys. Rev. B **68**, 134414 (2003).
[9] R. Kajimoto, H. Yoshizawa, H. Kawano, H. Kuwahara, Y. Tokura, K. Ohoyama, and M. Ohashi, Phys. Rev. B **60**, 9506 (1999).
[10] C. Cui, T. A. Tyson, Z. Chen, and Zh. Zhong, Phys. Rev. B **68**, 214417 (2003).
[11] R. C. Yu, J. Tang, L. D. Yao, A. Matsushita, Y. Yu, F. Y. Li, and C. Q. Jin, J. Appl. Phys. **97**, 083910 (2005).
[12] D. P. Kozlenko, V. P. Glazkov, Z. Jirák, and B. N. Savenko, J. Phys.: Condens. Matter **16**, 2381 (2004).
[13] I. Loa, P. Adler, A. Grzechnik, K. Syassen, U. Schwarz, M. Hanfland, G. Kh. Rozenberg, P. Gorodetsky, and M. P. Pasternak, Phys. Rev. Lett. **87**, 125501 (2001).
[14] A. Arulraj, R. E. Dinnebier, S. Carlson, M. Hanfland, and S. van Smaalen, Phys. Rev. Lett. **94**, 165504 (2005).
[15] N. A. Dubrovinskaia and L. S. Dubrovinsky, Rev. Sci. Instrum. **74**, 3433 (2003).
[16] A. P. Hammersley, S. O. Svensson, M. Hanfland, A. N. Fitch, and D. Hausermann, High Press. Res. **14**, 235 (1996).
[17] R. B. Von Dreele and A. C. Larson, Los Alamos National Labo-

ratory Report No. LAUR 86, 1986 (unpublished), p. 748.
[18] I. N. Goncharenko, V. P. Glazkov, A. V. Irodova, O. A. Lavrova, and V. A. Somenkov, J. Alloys Compd. **179**, 253 (1992); I. N. Goncharenko, High Press. Res. **24**, 193 (2004).
[19] I. N. Goncharenko, I. Mirebeau, P. Molina, and P. Boni, Physica B **234-236**, 1047 (1997).
[20] J. Rordíguez-Carvajal, Physica B **55**, 192 (1993).
[21] C. Meneghini, D. Levy, S. Mobilio, M. Ortolani, M. Nuñez-Reguero, A. Kumar, and D. D. Sarma, Phys. Rev. B **65**, 012111 (2001).
[22] F. J. Birch, J. Geophys. Res. **91**, 4949 (1986).
[23] L. Martín-Carrón, A. de Andrés, M. J. Martínez-Lope, M. T. Casais, and J. A. Alonso, Phys. Rev. B **66**, 174303 (2002).
[24] V. A. Amelitchev, B. Guttler, O. Yu. Gorbenko, A. R. Kaul, A. A. Bosak, and A. Yu. Ganin, Phys. Rev. B **63**, 104430 (2001).
[25] M. V. Abrashev, J. Bäckström, L. Börjesson, M. Pissas, N. Kolev, and M. N. Iliev, Phys. Rev. B **64**, 144429 (2001).
[26] E. Liarokapis, Th. Leventouri, D. Lampakis, D. Palles, J. J. Neumeier, and D. H. Goodwin, Phys. Rev. B **60**, 12758 (1999).
[27] D. P. Kozlenko, Z. Jirák, I. N. Goncharenko, and B. N. Savenko, J. Phys.: Condens. Matter **16**, 5883 (2004).
[28] A. Congeduti, P. Postorino, E. Caramagno, M. Nardone, A. Kumar, and D. D. Sarma, Phys. Rev. Lett. **86**, 1251 (2001).
[29] R. J. Angel, J. Zhao, and N. L. Ross, Phys. Rev. Lett. **95**, 025503 (2005).
[30] T. Tohei, A. Kuwabara, T. Yamamoto, F. Oba, and I. Tanaka, Phys. Rev. Lett. **94**, 035502 (2005).
[31] Z. Fang, I. V. Solovyev, and K. Terakura, Phys. Rev. Lett. **84**, 3169 (2000).
[32] K. H. Kim, S. Lee, T. W. Noh, and S. W. Cheong, Phys. Rev. Lett. **88**, 167204 (2002).
[33] S. Y. Park, Y. H. Hyun, Y. P. Lee, L. V. Svetchnikov, K. W. Kim, and V. G. Prokhorov, Appl. Phys. Lett. **89**, 052502 (2006).
[34] E. E. Rodriguez, Th. Proffen, A. Llobet, J. J. Rhyne, and J. F. Mitchell, Phys. Rev. B **71**, 104430 (2005).
[35] W. A. Harrison, *The Electronic Structure and Properties of Solids* (Freeman, San Francisco, CA, 1980).
[36] A. P. Ramirez, P. Schiffer, S. W. Cheong, C. H. Chen, W. Bao, T. T. M. Palstra, P. L. Gammel, D. J. Bishop, and B. Zegarski, Phys. Rev. Lett. **76**, 3188 (1996).
[37] R. Klingeler, J. Geck, S. Arumugam, N. Tristan, P. Reutler, B. Büchner, L. Pinsard-Gaudart, and A. Revcolevschi, Phys. Rev. B **73**, 214432 (2006).
[38] D. P. Kozlenko and B. N. Savenko, J. Phys.: Condens. Matter **16**, 9031 (2004).
[39] G. Venketeswara Pai, Phys. Rev. B **63**, 064431 (2001).
[40] J.-S. Zhou and J. B. Goodenough, Phys. Rev. B **68**, 054403 (2003).
[41] R. Mahendiran, S. K. Tiwary, A. K. Raychaudhuri, T. V. Ramakrishnan, R. Mahesh, N. Rangavittal, and C. N. R. Rao, Phys. Rev. B **53**, 3348 (1996).
[42] G. Zhao, K. Conder, H. Keller, and K. A. Müller, Nature (London) **381**, 676 (1996).
[43] H. Aliaga, D. Magnoux, A. Moreo, D. Poilblanc, S. Yunoki, and E. Dagotto, Phys. Rev. B **68**, 104405 (2003).
[44] O. Cépas, H. R. Krishnamurthy, and T. V. Ramakrishnan, Phys. Rev. Lett. **94**, 247207 (2005).
[45] L. Brey, Phys. Rev. B **71**, 174426 (2005).
[46] J. vandenBrink, G. Khaliullin, and D. Khomskii, Phys. Rev. Lett. **83**, 5118 (1999).
[47] G. Jackeli, N. B. Perkins, and N. M. Plakida, Phys. Rev. B **62**, 372 (2000).
[48] I. V. Solovyev and K. Terakura, Phys. Rev. Lett. **83**, 2825 (1999).